An Innovative Analog Circuit to Retrieve Energy Information from Signals of Deeply Saturated Pre-Amplifiers Connected to Semiconductor Detectors

Stefano Capra, Giacomo Secci, Alberto Pullia

***Abstract*—In nuclear spectroscopy by definition a distorted signal from a saturated pre-amplifier cannot contain the correct energy information, being this one directly related to the signal amplitude. In this work we propose an innovative technique to exploit the charge-conservation principle to extract high-resolution energy information from a deeply saturated charge-sensitive pre-amplifier connected to semiconductor detectors. The previously described "Fast-Reset" technique enables to reconstruct the energy information from a saturated preamplifier collecting the charge on the input node with a current generator and performing a time-over-threshold measurement. However it requires an off-line post processing of the acquired data. The proposed circuit, instead, requires no post processing thanks to a peculiar Time-to-Amplitude converter that integrates a baseline rejection circuit. In this way an extension of the pre-amplifier spectroscopic energy range of a factor 20 or more is possible, with the generation of a signal whose shape is optimized for direct acquisition with a pulse-height analyzer and no additional filtering.**

I. Introduction

Nuclear spectroscopy with semiconductor detectors turns out in most cases to be a pulse amplitude spectroscopy [1], [2], [3]. The charge released by the detector due to the interaction with the impinging radiation is proportional to the energy deposited inside the crystal. Such charge is turned into voltage by pre-amplifiers, which are typically active integrators. The pre-amp output is passed through one or more filters, analog or digital, and the resulting pulse height is measured and put into an histogram. After proper calibration, the pulse height is associated with a specific energy. In a well designed spectroscopic chain there is a linear correspondence between radiation energy at the input and signal amplitude at the output. This linearity is guaranteed, according to the limits of the electronics, up to the level of saturation of one or more of the elements of the signal chain. In case of saturation the law of direct correlation between signal amplitude and radiation energy is broken and the information is corrupted.

VLSI solutions are mandatory for very dense applications, but technology scaling has the drawback of reduction in CMOS breakdown voltages. In a charge-sensitive pre-amplifier (CSP) the only scale factor between the charge released by the detector and the corresponding output voltage amplitude is the value of the feedback capacitor (C_F). Given an available output voltage swing, limited only by the power rails, the conventional pre-amplifier maximum spectroscopic energy range E_{dyn} is determined by the equation

$$E_{dyn} = k \cdot C_F \cdot V_{SAT} \tag{1}$$

where V_{SAT} is the pre-amplifier saturation voltage and k is the proportionality factor between the energy deposited in the detector (E_{DET}) and the released charge (Q_{DET}). In an attempt to increase such range, the circuit designer can increase C_F, but this comes at the price of lowering the pre-amplifier gain and worsening the noise performance of the circuit. In other words, there is no trivial solution to increase the conventional dynamic range of a charge-sensitive pre-amplifier.

It is also worth mentioning another issue connected to dynamic range limitations. When a charge pre-amplifier saturates it is not able to process any other incoming signal from the detector, introducing a "dead time", which spans from the beginning to the end of the saturation condition. In continuous reset architectures, when the pre-amplifier works in its linear range, after each event the output signal goes back to the quiescent voltage with a time constant defined by the feedback resistor, R_F, and capacitor, C_F. However, in case of saturation, the dead time can last much longer than this. In fact, it can last up to few milliseconds in pre-amplifiers both for γ spectroscopy [4] and for particle/ion detectors [5]. The reason is the following: while the output signal is saturated, due to the excess of charge Q_{EXC}, the feedback resistor generates a constant current, I_F, equal to the saturation voltage divided by the value of the feedback resistance. This is a simple application of the Ohm's law considering, for simplicity, a pre-amplifier input operating point of 0 V and a negligible input voltage bounce. In the approximation of zero baseline before saturation, the dead time formula is the following:

$$deadtime = \frac{Q_{EXC}}{I_F} = \frac{E - E_{dyn}}{k} \frac{R_F}{|V_{SAT}|} = \frac{E - E_{dyn}}{E_{dyn}} \cdot R_F C_F \tag{2}$$

where E is the event energy, E_{dyn} is the conventional dynamic range of the pre-amplifier, k is the same proportionality factor shown in equation (1) and V_{SAT} is the saturation voltage of the pre-amplifier with respect to the zero-level reference.

S. Capra is with the Department of Physics, University of Milan and INFN of Milan, Italy (email: stefano.capra@unimi.it).

G. Secci was with the Department of Physics, University of Milan and now is with INFN of Milan, Italy (email: giacomo.secci@mi.infn.it).

A. Pullia is with the Department of Physics, University of Milan and INFN of Milan, Italy (email: alberto.pullia@mi.infn.it).

Essentially the ratio between the excess charge and the maximum processable charge is a multiplication factor of the pre-amplifier time constant in determining the dead time duration.

A common solution to the dead time problem is the implementation of a controlled switch in parallel to the feedback resistor that can swiftly reset the pre-amplifier in case of saturation [6]. The extension of the conventional dynamic range is generally achieved with variable-gain systems with switchable feedback capacitors [7]. In this paper we propose a solution that solves the dead time issue while simultaneously allowing for conventional low-energy spectroscopy within the CSP's saturation limit and for high-resolution spectroscopy up to roughly 20 times the conventional dynamic energy range of the circuit. With a time-over-threshold technique it is in fact possible to retrieve the energy of an event that caused pre-amplifier saturation with resolution and accuracy compatible with the requisites of γ spectroscopy [8], i.e. in the order of 0.1%, without this measurement being affected by the pre-amplifier baseline fluctuations. Such solution has been implemented in an integrated circuit realized in AMS C35 technology and extensively tested.

There are various experimental contexts where this kind of circuit would be extremely useful. A first possible application concerns the experiments in which HPGe detectors are not only used to perform usual 1-8 MeV γ spectroscopy but also to detect highly energetic cosmic radiation [9], [10]. Such work makes use of the state-of-the-art AGATA pre-amplifier that implements a Time-Over-Threshold (ToT) method applied to the pre-amplifier's second stage and that relies on the linearity of the first one. The proposed circuit can be considered an evolution of such pre-amplifier, because the effectiveness of the fast-reset energy measurement is not affected by the pre-amp first-stage saturation. A further use concerns the decay spectroscopy experiments. In this context, beams with energies up to 100 MeV/nucleon are stopped, with a huge energy release, in the very same silicon detectors [11] used to monitor the α or β decay in the 5-8 MeV energy range. The time difference between implantation and decay goes from the tens-of-microseconds up to the millisecond range in the case of exotic nuclei. The proposed circuit can be used to measure both implantation and decay energies with high resolution and linearity instead of using logarithmic amplifiers. In this application the required energy range goes from 150 keV up to several hundreds of MeV. Finally it is interesting to consider the nuclear physics experiments where beams used for nucleon transfer reactions may have energies up to 50-100 MeV/nucleon. After the reaction the ions generally continue their path at 0 degrees. The reactions leave behind as residuals some light particles with energy that depends not only on the beam one but also on the target nuclear species. These particles can easily have an energy of few hundreds of MeV and its measurement with silicon detectors [12] allows to extract quantum numbers of the populated state. In the same experiments it is often requested to perform high-resolution spectroscopy on light particles emitted with much lower energy, i.e. in the 5-40 MeV range.

II. Circuit description

The basic functionality of the circuit relies on the physical principle of the conservation of the charge, which states that in an isolated system, the total electric charge never changes. Except for the feedback resistance, which effect is negligible, the input node is isolated, because it is only connected to capacitive elements tied to ground. When the pre-amplifier is operating in a conventional mode, the charge released by the detector in the short term is collected by the feedback capacitor and in the long term is removed from it by the feedback resistor, being it discrete [13], [14], integrated [15], [16] or made by an active trans-conductor [17]. The amplitude of the output signal is proportional to the amount of charge collected: for this reason the information about the radiation energy is retrieved performing amplitude spectroscopy on the output signals.

When a highly energetic radiation interacts with the detector and generates a quantity of charge that is superior to the one the pre-amplifier is able to handle, the output voltage reaches the edge of its available swing, the resulting signal becomes distorted and the energy information corrupted. The charge released by the detector, however, if there are no parasitic leakage paths, stays trapped on the stray capacitors of the pre-amplifier input node. So it is still possible to collect and measure it by using an adequate circuit, as described below.

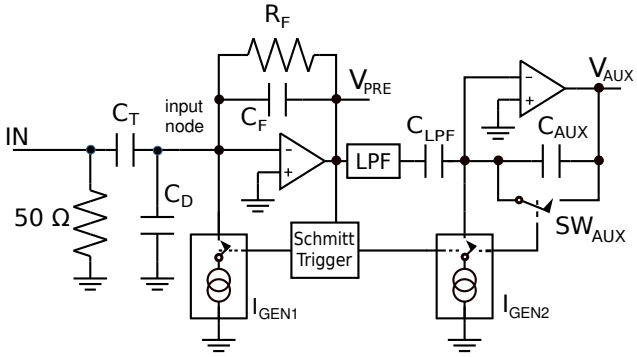

Fig. 1. Schematic diagram of the integrated charge-sensitive pre-amplifier with fast-reset device and time-to-amplitude converter [18]. A simple injection circuit, shown on the left, to be connected to a pulser, allows to simulate the detector impedance and the signal.

The circuit structure is shown in Fig. 1. The core of the circuit is a low-noise integrated charge-sensitive pre-amplifier [19] that works as first stage. For energies under the saturation threshold this pre-amplifier works in a conventional way. Its signals are meant to be processed with analog or digital shaping filters in order to perform spectroscopy with 130 electrons RMS of resolution.

This pre-amplifier is equipped with a fast-reset circuit [20] that is activated in case of saturation, i.e. for energies above roughly 40 MeV. The saturation condition is monitored with a comparator configured as Schmitt trigger: when the output voltage crosses the first pre-defined threshold V_{th1} the reset feature starts and ends only when it crosses a second threshold V_{th2}, close to the pre-amplifier quiescent point. The thresholds V_{th1} and V_{th2} are determined by the supply voltage value and the ratio of the resistors that make up the Schmitt trigger. As

described in the next paragraphs, this method is robust, i.e. it is able to cancel the tail-to-pulse pileup, or the effect of any random value of the pre-pulse baseline. The reset feature is obtained with a current generator (labelled I_{GEN1} in Fig. 1) connected to the input node of the pre-amplifier: its role is to drain all the excess charge in a controlled manner.

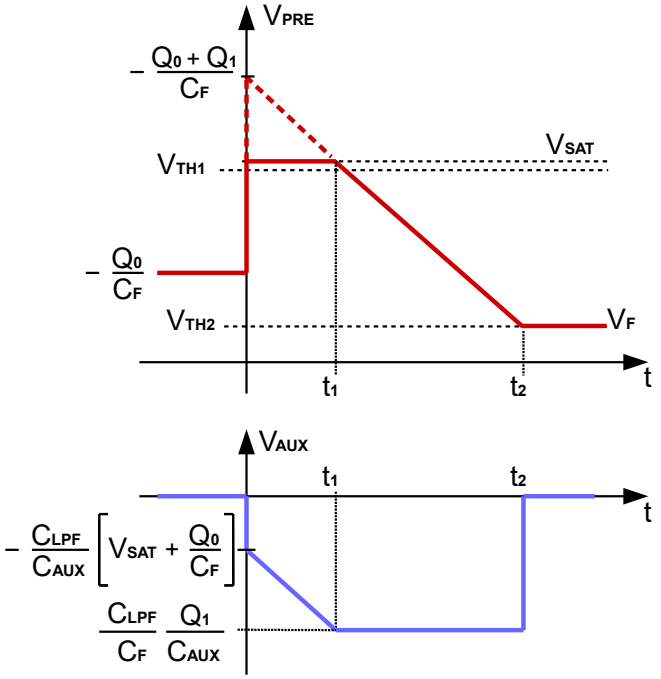

Fig. 2. Schematic representations of the two output signals of the proposed circuit: the pre-amplifier output and the auxiliary output. Q_0 and Q_1 are assumed to be negative, which yields the positive sign for $-Q_0/C_F$ and $-(Q_1+Q_0)/C_F$.

The circuit behaviour is summarized in Fig. 2. In the initial condition the pre-amplifier output voltage is at some baseline with value $-Q_0/C_F$. The negative sign is due to the inverting configuration of the pre-amplifier. At $t=0$ a highly energetic event releases a charge Q_1 that exceeds the saturation threshold of the pre-amplifier. Assuming that Q_1 is negative, the output signal starts to rise and crosses at first V_{th1} activating the fast-reset and, some nanoseconds after, hits the saturation level V_{SAT}. During the fast-reset phase, the current generator I_{GEN1} switches on drawing the current I_{res1}, as described in the following equation:

$$I_{GEN1}(t) = \begin{cases} 0 & t \le 0 \\ I_{res1} & 0 < t \le t_2 \\ 0 & t > t_2. \end{cases} \tag{3}$$

The output voltage stays in saturation until the reset circuit has removed enough charge from the input node to allow the pre-amplifier to come back in its linear condition ($t=t_1$). After t_1 the output signal moves towards the natural pre-amplifier quiescent point with a fixed slope of I_{res1}/C_F, given by the law of the capacitor. The exact circuit behaviour in proximity of t_1 cannot be easily determined, because in that instant the circuit is exiting the saturation condition and the feedback loop is closed again. A detailed description of how to deal with this phenomenon is elaborated in section III-D. As soon as the output signal crosses V_{th2} the current generator is de-activated, the reset phase ends and the pre-amplifier operates in its conventional way again. The effect of the feedback resistor is negligible because the associated time constant $R_F C_F$ is typically orders of magnitude longer than the reset phase. The circuit behaviour is summarized in (4).

$$V_{PRE}(t) = \begin{cases} -\dfrac{Q_0}{C_F} & t \le 0 \\ V_{SAT} & 0 < t \le t_1 \\ -\dfrac{I_{res1}}{C_F}t - \dfrac{Q_0+Q_1}{C_F} & t_1 < t \le t_2 \\ V_F & t > t_2 \end{cases} \tag{4}$$

Given the quantities Q_0, Q_1, I_{res1}, V_{th1}, V_{th2} and V_{SAT} we can find t_1 and t_2. The most straightforward way to calculate t_1 is to imagine the behaviour of an ideal pre-amplifier with infinite dynamic range (dashed line in Fig. 2) and neglecting the charge collection time. The ideal signal would start from $-(Q_0+Q_1)/C_F$ with descending slope I_{res1}/C_F. The intersection with $V=V_{SAT}$ gives the value of t_1.

$$t_1 = -\frac{Q_0+Q_1+C_F V_{SAT}}{I_{res1}} \tag{5}$$

$$t_2 = -\frac{Q_0+Q_1+C_F V_F}{I_{res1}} \tag{6}$$

As can be seen from equation (6), if we measure only the total reset time t_2 we are unable to disentangle Q_0 and Q_1. Signal charge Q_1 can however be derived by properly processing (6) and the pre-pulse baseline $-Q_0/C_F$. A digital off-line implementation of such a processing algorithm has already been proposed and verified [21]. The solution proposed here implements such algorithm automatically and in real time with no need of off-line post processing.

It is now possible to calculate the response of the auxiliary circuit. This one can be seen as a time-to-amplitude converter (TAC) which integrates the current of I_{GEN2} (equal to $I_{res2} = I_{res1}$ during reset and equal to 0 in any other case) on the capacitor C_{AUX} during the reset phase. A dedicated switch SW_{AUX} ensures that the output of this circuit is zero whenever the reset is de-activated. The peculiarity of this circuit is the ability to separate the contribution of Q_0 from the one of Q_1 in the measurement of (6), providing an analog output pulse V_{AUX} whose height depends on Q_1 only.

The current I_{AUX} integrated on the auxiliary capacitor C_{AUX} during the reset phase is given by the sum of the current I_{LPF} flowing through the capacitance C_{LPF} and the current I_{res2} of the second generator. We can neglect for the moment the effect of the low-pass filter (LPF) block and imagine to drive directly C_{LPF} with the pre-amplifier output.

$$I_{AUX} = I_{res2} + I_{LPF} = I_{res2} + C_{LPF}\frac{dV_{PRE}}{dt} \tag{7}$$

with

$$\frac{dV_{PRE}}{dt}(t) = \delta(t)\cdot\left(V_{SAT}+\frac{Q_0}{C_F}\right) - \theta(t-t_1)\cdot\frac{I_{res1}}{C_F} \tag{8}$$

where δ indicates the Dirac delta function, while θ indicates the Heaviside step function. Considering that $dV_{AUX}/dt = -I_{AUX}/C_{AUX}$, we can find the auxiliary device output voltage:

$$\begin{aligned} V_{AUX}(t) &= -\frac{1}{C_{AUX}}\int_0^t \left[I_{res2} + C_{LPF}\frac{dV_{PRE}(\tau)}{d\tau} \right] d\tau \\ &= -\frac{I_{res2}}{C_{AUX}}t - \frac{C_{LPF}}{C_{AUX}}[V_{PRE}(t) - V_{PRE}(0)] \end{aligned} \tag{9}$$

We can expand the expression in (9) using the information in (4), obtaining (10).

$$V_{AUX}(t) = \begin{cases} 0 & t \le 0 \\ -\frac{I_{res2}}{C_{AUX}}t - \frac{C_{LPF}}{C_{AUX}}\left(V_{SAT} + \frac{Q_0}{C_F}\right) & 0 < t \le t_1 \\ -\frac{t}{C_{AUX}}\left[I_{res2} - \frac{C_{LPF}}{C_F}I_{res1}\right] + \frac{C_{LPF}}{C_F}\frac{Q_1}{C_{AUX}} & t_1 < t \le t_2 \\ 0 & t > t_2 \end{cases} \tag{10}$$

For $t < 0$ and $t > t_2$, $V_{AUX} = 0$ because the switch in parallel with the capacitor C_{AUX} is closed and the auxiliary device works as a ground-follower. Between $t = 0$ and $t = t_1$ the auxiliary signal rises. By design C_{LPF} is chosen to be equal to C_F and $I_{res1} = I_{res2}$. These conditions cancel out the dependency of V_{AUX} from the time between t_1 and t_2, resulting in a flat-topped auxiliary output pulse. From (10) we can conclude that such flat top has an amplitude V_{FT} equal to:

$$V_{FT} = \frac{C_{LPF}}{C_F}\frac{Q_1}{C_{AUX}} \tag{11}$$

The same conditions that ensure that the derivative of V_{AUX} is zero between t_1 and t_2 guarantee that no contribution from Q_0 can affect the value of V_{FT}. Since this relies both on the fact that $C_{LPF} = C_F$ and that $I_{res1} = I_{res2}$, it is necessary to add the possibility to fine-tune I_{res2} in order to address the issues possibly introduced by asymmetries between the circuit components during fabrication. A dedicated external trimmer or internal variable resistor adjusted via digital slow control can correct for such mismatches. The stability of the two current generators I_{GEN1} and I_{GEN2} in this circuit is paramount to achieve the desired linearity and resolution.

Note that looking at (7), in order I_{AUX} to be correctly integrated on C_{AUX}, it is necessary that the pre-amplifier voltage step at $t = 0$ is sampled correctly by C_{LPF}. This is in principle not possible because SW_{AUX} is opened only once the pre-amplifier voltage has reached V_{SAT}. The pre-amplifier itself has a rise-time typically between 10 and 150 ns. For this reason C_{LPF} is not driven directly by the pre-amplifier output but from the low-pass filter block. Apart from smoothing the pre-amplifier noise, this filter has the role of delaying the value of the pre-amplifier baseline for several nanoseconds so that when the pre-amplifier signal crosses V_{th1} and the reset starts, this filter is still at a voltage level in first approximation equal to $-Q_0/C_F$ as shown in Fig. 3. In order the algorithm to work properly, the time constant of this low-pass filter should be longer than the pre-amplifier rise-time and shorter than $t_2 - t_1 = (V_{SAT} - V_F) \cdot C_F/I_{res1}$. As long as these conditions are met, it can be demonstrated that the effect of the low-pass filter on the auxiliary circuit behaviour is negligible and the net effect on (10) is just a constant additional term that is canceled out during calibration. Given the short time constant, this filter can be implemented in an integrated circuit just with passive components, with C_{LPF} as the last capacitor of a properly sized RC chain.

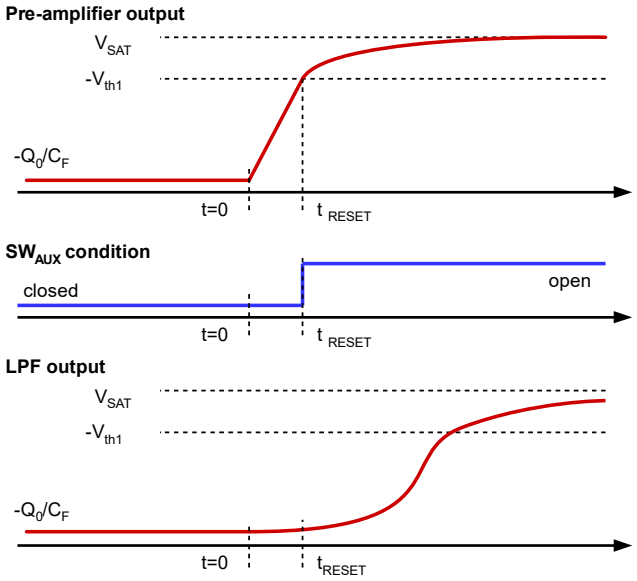

Fig. 3. Detail of the beginning of the reset phase. The pre-amplifier output, the switch SW_{AUX} condition and the output of the low-pass filter block are reported.

It should be pointed out that, since during the fast-reset procedure the pre-amplifier is saturated, the leading-edge signal shape may be too distorted to be used to perform pulse-shape analysis [22], [23].

III. Circuit Characterization

This analog algorithm has been implemented in an integrated charge-sensitive pre-amplifier realized in AMS C35 technology. The chip is powered with ± 2.5 V and the overall power consumption is around 22 mW. The pre-amplifier is able to drive a terminated coaxial line with an available positive voltage swing of roughly 2 V. The chip was packaged in a JLCC68 carrier and mounted on a custom-designed PCB. The detector was simulated with a pulser connected to the input node of the pre-amplifier through the injection circuit. A test capacitor of alternatively 3.8 pF or 4.3 pF was used. The reset threshold of the CSP is slightly under 40 MeV in germanium, roughly equivalent to 2 pC.

A. Linearity

In order to test the linearity of the proposed circuit, a step voltage from 0.5 V to 9 V and with rise time of 3 ns was provided to a 4.3 pF test capacitor. In this way it was possible to achieve charge pulses from 2.15 pC to 38.7 pC, corresponding to energies from 40 MeV to 717 MeV in germanium or from 49 MeV to 880 MeV in silicon. The pulser frequency was set sufficiently low, 9 Hz, so that the pre-amplifier signal tail from an event could be completely suppressed before

TABLE I
RESULTS OF THE LINEARITY TEST PERFORMED ON THE AUXILIARY CIRCUIT'S OUTPUT.

INPUT				OUTPUT			
Vtest [mV]	**Q_1 [pC]**	**Energy [MeV in Ge]**	**Energy [MeV in Si]**	**Aux pulse height [mV]**	**Best fit [mV]**	**Absolute residual [mV]**	**Relative residual [%]**
500	2.15	40	49	-114.5	−114.38	−0.12	0.10
1000	4.3	80	98	-225.5	−225.18	−0.32	0.14
2000	8.6	159	196	-445.6	−446.76	1.16	−0.26
3000	12.9	239	293	-668.6	−668.35	−0.25	0.04
4000	17.2	318	391	-889.4	−889.93	0.53	−0.06
5000	21.5	398	489	-1112	−1111.52	−0.48	0.04
6000	25.8	477	587	-1335	−1333.10	−1.90	0.14
7000	30.1	557	685	-1558	−1554.69	−3.31	0.21
8000	34.4	636	783	-1783	−1776.28	−6.72	0.38
9000	38.7	716	880	-2009	−1997.86	−11.14	0.55

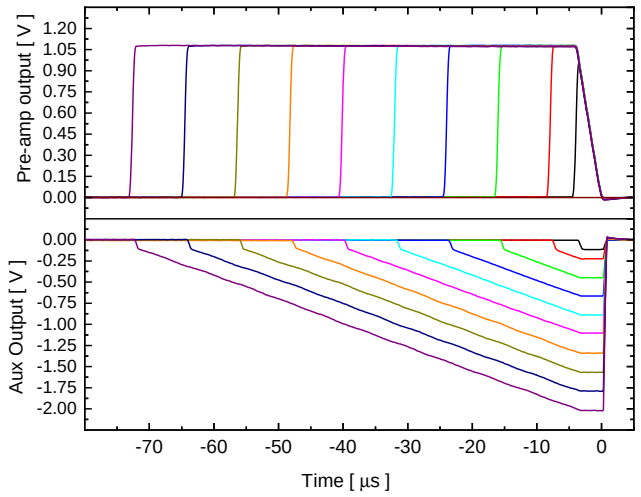

Fig. 4. Output signals produced by the auxiliary device after the injection of test charge pulses Q_1 from 2.15 pC to 38.7 pC

the beginning of the following one. In fact, using a square-wave pulser, it is unavoidable to inject alternatively charge signals with opposite polarity. Being the fast-reset circuit able to process only signals with a specific polarity, the opposite ones actually cause saturation that induce a dead-time and a signal tail with duration in the order of few milliseconds. The output waveforms of the CSP and the pulses seen at the auxiliary device output were acquired with a 5 GS/s, 500 MHz digital oscilloscope. During the data acquisition the vertical scale of the oscilloscope was kept constant in order to avoid fictious non-linearities due to non homogeneous scope scale references.

In Fig. 4 signals from the pre-amplifier and the auxiliary circuit are shown. As can be seen, the saturated pre-amplifier pulses have different duration according to the amount of the incoming charge. The auxiliary pulses are as expected in Fig. 2, with a height proportional to the injected charge Q_1. This figure is taken using the end point of the reset procedure as trigger time, so that the pre-amplifier trailing edges, and thus the auxiliary flat-tops, are aligned.

The height of the auxiliary signals was measured with the scope at t =−2.5 µs, i.e. approximately in the middle of the flat-top. Such values are reported in Table I. The linear fit, performed with the weighted least squares algorithm, shows an excellent data linearity, with residuals mostly lower than 0.1%, with a worst case of 0.55% at high energy. We define residual as the difference between experimental amplitude and fit line, divided by the value of the experimental amplitude itself.

B. Resolution

The next step in the circuit characterization is the evaluation of the resolution associated to the charge measurement with this technique. For the same test pulses and test capacitor used to characterize the circuit linearity, the corresponding Root-Mean-Square (RMS) pulse height fluctuations σ_{height} were measured, each on a dataset of 100 repetitions. The results are reported in Table II.

The total signal height fluctuation σ_{height} is the sum of two contributions. The first (σ_{eff}) is the effective signal amplitude fluctuation due to the noise of the circuit under characterization. The second (σ_{scope}) is the uncertainty introduced by the scope noise. For this reason σ_{eff} is obtained subtracting in quadrature the scope noise from the experimental value, as in the following equation:

$$\sigma_{eff} = \sqrt{{\sigma_{height}}^2 - {\sigma_{scope}}^2}. \quad (12)$$

TABLE II
RESULTS OF THE RESOLUTION TEST PERFORMED ON THE AUXILIARY CIRCUIT'S OUTPUT. ALL σ VALUES ARE EVALUATED AS RMS (ROOT-MEAN-SQUARE) FLUCTUATIONS.

Q_1 [pC]	σ_{height} [mV]	σ_{scope} [mV]	σ_{eff} [mV]	σ_Q [fC]	Res. FWHM [%]
2.15	0.15	0.05	0.14	2.6	0.29
4.3	0.13	0.05	0.12	2.2	0.12
8.6	0.22	0.05	0.21	4.1	0.11
12.9	0.27	0.05	0.27	5.1	0.09
17.2	0.18	0.05	0.17	3.3	0.05
21.5	0.51	0.43	0.27	5.3	0.06
25.8	1.15	0.96	0.63	12.2	0.11
30.1	1.34	0.96	0.93	18.1	0.14
34.4	1.34	0.96	0.93	18.1	0.12
38.7	1.46	0.96	1.10	21.2	0.13

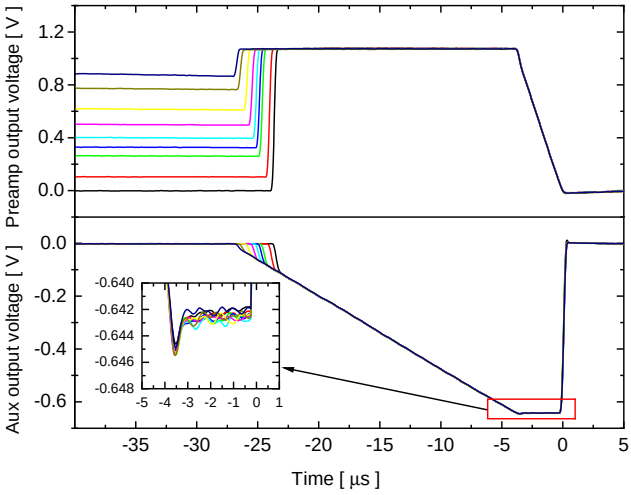

Fig. 5. Signals produced by the auxiliary circuit during reset phases induced by events of roughly 11.6 pC. A baseline fluctuation of maximum amplitude 1.52 pC is highlighted in the inset.

The intrinsic scope signal fluctuation σ_{scope} depends on the acquisition scale set: 5, 100 or 200 mV/div. For every measurement the scope noise is reported. The uncertainty σ_Q associated to the charge measurement was calculated using the calibration factor extracted from the linear fit on the dataset presented in the previous section. The worst measured resolution of 0.29% FWHM (Full Width at Half Maximum) is obtained with the smallest charge injection ($Q_1 = 2.15$ pC). This value rapidly improves up to the best-case resolution of 0.05% FWHM, measured with a charge pulse of approximately 17 pC. The FWHM resolutions are less than 0.15%, which is an excellent result in the context of the spectroscopy experiments for which the proposed circuit has been designed.

C. Baseline rejection

As discussed in section II, the duration of a fast-reset event is proportional to the sum of the charge Q_1 released by the detector during the event that causes saturation and the baseline charge Q_0. The fundamental feature of the proposed circuit is to provide analog pulses with height proportional to Q_1 only, canceling the contribution from Q_0. In order to evaluate the baseline rejection capability, the pulser was programmed to provide a double step signal. In this way two closely spaced charge pulses of controlled amplitudes were generated. The first one was used to set a baseline value at the pre-amplifier output and the second was used to simulate a saturating event. A set of 7 Q_1 values from 3.9 pC to 27.2 pC was chosen. For each of these values, the auxiliary output signal amplitude was measured with a set of baseline values between zero (CSP on its quiescent point) and a maximum baseline equivalent to 80% of the full CSP voltage swing. The charge difference ΔQ_0 on the input node between the maximum and minimum baseline conditions can be calculated knowing the value of the feedback capacitor (0.88 pF) and is equivalent to 1.52 pC. In Fig. 5 the auxiliary circuit output signals corresponding to the dataset with Q_1 =11.64 pC are

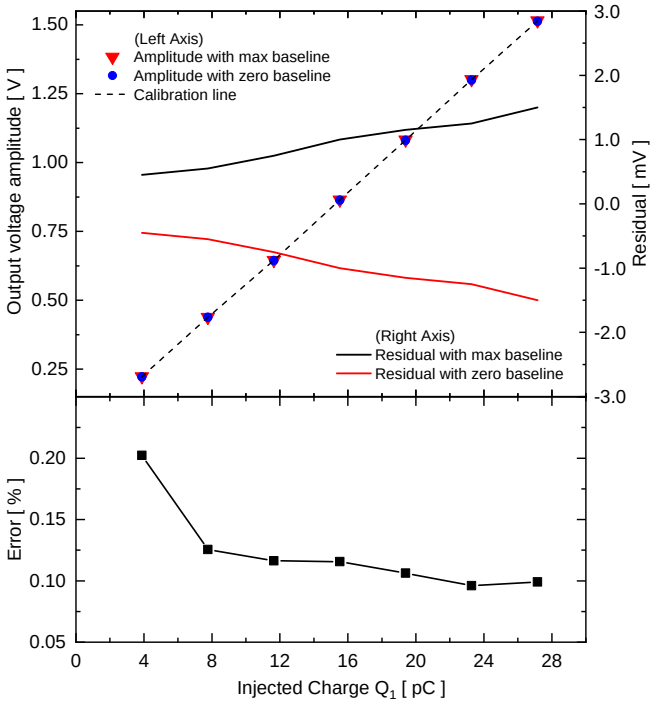

Fig. 6. *Top figure*: output voltage amplitudes from the auxiliary device with maximum baseline and with zero baseline (left axis). Difference between the amplitude measurements with maximum baseline (black) or with zero baseline (red) and their average (right axis). *Bottom figure*: maximum percentage error on the voltage amplitude measurements.

shown. The height of such signals, as measured with an oscilloscope, is actually constant and not dependent on the pre-pulse baseline, which confirms the effectiveness of the proposed circuit.

The full dataset is plotted in Fig. 6, in which the system was calibrated on the signal amplitudes obtainable with a baseline equal to 50% of the available CSP voltage swing. The deviation of the charge measurement induced by the maximum possible baseline fluctuation is always equal or lower than ±0.20% (worst case obtained with the smallest charge injection of 4 pC), with this value falling to ±0.1% for injected charges Q_1 equal or larger than 8 pC.

In Tab III the baseline rejection measurements are summarized. We define ΔQ_{AUX} as the portion of the residual charge on the input node due to the presence of baseline that "leaks"

TABLE III
RESULTS OF THE BASELINE REJECTION TEST PERFORMED ON THE AUXILIARY CIRCUIT'S OUTPUT.

Q_1 [pC]	ΔQ_0 [pC]	ΔQ_{AUX} [fC]	Rejection percentage [%]
3.88	1.52	16	99
7.76	1.52	20	99
11.64	1.52	27	98
15.52	1.52	36	98
19.40	1.52	41	97
23.28	1.52	45	97
27.16	1.52	54	96

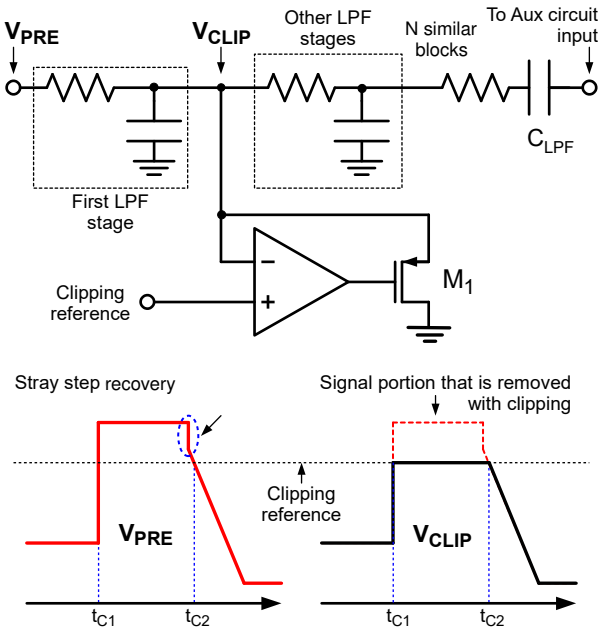

Fig. 7. Simplified schematic of the clipping circuit used to remove the pre-amplifier artifacts from the auxiliary output signal. A P-MOS transistor is inserted in the negative feedback path of an op-amp and limits the positive swing of the signal under a pre-defined clipping reference.

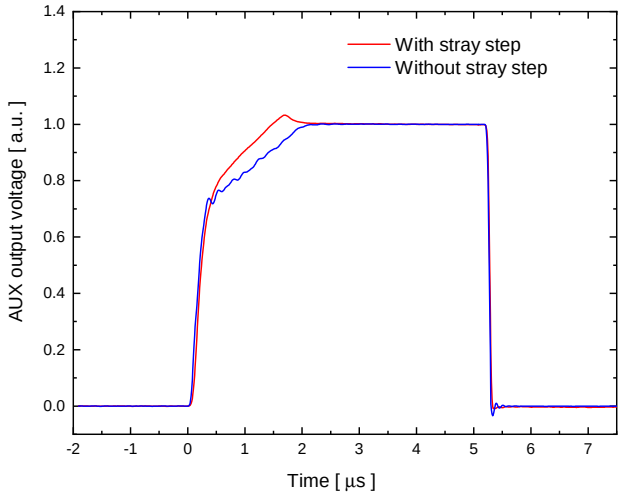

Fig. 8. Comparison of normalized aux output pulses from the two circuits: one without the step removal and one with the step removal circuit. In the latter the ripple on the top of the signal is evidently removed. Such pulse can be directly fed into a pulse-height analyzer for amplitude spectroscopy.

through the auxiliary circuit. The baseline charge rejection percentage is between 96% and 99%. It should be underlined that, given the pre-amplifier voltage swing, the maximum stray charge Q_0 is around 1.5 pC. The 4% of this charge, i.e. the quantity that is not rejected and that leaks in the measurement (61 fC), is clearly negligible with respect to the charge being measured (27 pC), constituting only the 0.2% of it.

D. Stray step removal

The pre-amplifier output signals show a peculiar non-ideality, or a ripple at the beginning of the negative constant-slope reset decay. In this corner point the negative feedback loop is abruptly closed and the op-amp starts working as a charge integrator again. Due to such regime switch, a stray negative voltage of approximately 200 mV shows up at the pre-amplifier output. This is caused by the circuit structure of the output stage, designed to drive a terminated 50 Ω coaxial line. The net result of this phenomenon as seen at the output of the auxiliary TAC circuit is the presence of a small ripple at the beginning of the pulse's flat-top, as shown in Fig. 5. This ripple may have detrimental effects on the resolution when reading out the TAC pulses with a pulse-height analyzer.

The proposed solution, able to remove this ripple, is shown in Fig. 7. The idea is to feed a clipped version of the pre-amplifier output signal (V_{CLIP}) into the TAC block. The goal of this clipping is to cut out the signal portion containing the stray step. A clipping circuit consisting of a P-MOS transistor (M_1) and an op-amp is connected immediately after the first R-C stage of the low-pass filter. Transistor M_1 keeps voltage V_{CLIP} always under a pre-defined clipping reference. In this way the signal portion containing the step is truncated and not sent to the auxiliary TAC circuit. M_1 is shut off whenever the signal is under such threshold. The clipping circuit shouldn't affect the auxiliary output signal neither before the beginning of saturation nor during the constant-slope decay. This aspect is paramount, since the clipping circuit must have no effect during both the baseline sampling and the TAC pulse's flat-top.

The fact that the clipping operation has no effect on the charge measurement can be easily deduced from (9). Let's define t_{C1} and t_{C2} respectively as the times at the beginning and at the end of the clipping (see Fig. 7). Substituting in (9) V_{PRE} with V_{CLIP} the integrals of $dV_{PRE}/d\tau$ and $dV_{CLIP}/d\tau$ between t_{C1} and t_{C2} are both identically null since since $V_{PRE}(t_{C2}) = V_{PRE}(t_{C1})$ and $V_{CLIP}(t_{C2}) = V_{CLIP}(t_{C1})$. The value of V_{AUX} for $t_{C2} < t < t_2$ is thus unaffected by this operation. The clipping has also no effect on the pre-amplifier output signal because it is performed inside the LPF block: it only limits the maximum baseline level the TAC circuit is able to correctly process.

The clipping effect on the TAC output signal shape is clearly visible in Fig. 8. In this figure the TAC pulses from two circuit versions are shown. The red signal comes from the original circuit, while the blue one comes from an improved version, equipped with the clipping circuit. The voltage ripple is effectively removed while leaving the flat-top unchanged, and thus the charge measurement is not affected.

IV. Conclusions

In this work a technique to retrieve the energy of events that saturate the pre-amplifier is presented: it is an evolution of the Fast-Reset technique previously described in literature. It is realized in the form of an auxiliary circuit that can be tied to a pre-amplifier equipped with fast-reset device. The biggest improvement is constituted by the ability to retrieve energy information without it being affected by the pre-amplifier baseline value. This analog real-time algorithm has been implemented in an ASIC pre-amplifier realized in AMS C35B4C3 technology with a saturation threshold of roughly

2 pC. The maximum measurable charge is around 28 pC: this limit is imposed by the voltage bounce on the pre-amplifier's input node: larger charge injections can activate the input-stage protection diodes, resulting in charge loss. The energy resolution obtainable with this device is better than 0.3% FWHM. The circuit, in the worst condition of signal-to-noise ratio, is able to remove 99% of the baseline charge from the measurement. An additional circuit was presented to mask the transient effects produced by the pre-amplifier during the transition from saturation to linear operation, so that they don't leak into the waveform produced by the auxiliary circuit.

It has been demonstrated that a pre-amplifier equipped with the described auxiliary circuit can perform high-resolution spectroscopy above its own saturation threshold. The maximum charge the circuit can correctly measure is 20 times or more larger than the one that naturally saturates the CSP. The 0.3% FWHM resolution in the extended energy range, unaffected by tail-to-pulse pile-up, can be considered a remarkable and innovative result.

When using this circuit in combination with a low-noise charge-sensitive pre-amplifier, it is possible to perform high-resolution spectroscopy for non-saturated signals according to the noise performance of the CSP itself. At the same time this circuit opens up the possibility to retrieve the energy information of high-energy deeply-saturated events with high accuracy. The pre-amplifier output and the auxiliary output are meant to be acquired simultaneously and processed with two different signal chains. The events under the saturation threshold do not produce any signal on the auxiliary output: they produce conventional exponential pulses on the pre-amplifier output that must be filtered with analog or digital shaping amplifiers/algorithms. The high-energy events that cause saturation are processed by the auxiliary circuit that outputs analog pulses with amplitude proportional to the collected charge. Joining the information coming from the two spectra (from CSP and from auxiliary circuit) it is possible to obtain a complete energy spectrum that extends orders of magnitude beyond the conventional CSP dynamic energy range limit.

By engineering the circuit in such a way that the polarity and the range of the auxiliary signals are the same as those of the pre-amplifier, one could in principle multiplex the two signals on the same physical line and acquire the mixed information with a single digitizer or analog memory [24] channel.

REFERENCES

[1] A. Goasduff *et al.*, "The GALILEO gamma-ray array at the legnaro national laboratories," *Nucl. Instrum. Methods Phys. Res. A: Accel. Spectrom. Detect. Assoc. Equip.*, vol. 1015, 2021.

[2] S. Akkoyun *et al.*, "AGATA—Advanced GAmma Tracking Array," *Nuclear Instruments and Methods in Physics Research Section A: Accelerators, Spectrometers, Detectors and Associated Equipment*, vol. 668, pp. 26–58, 2012.

[3] J. J. Dormard *et al.*, "Pulse shape discrimination for GRIT: Beam test of a new integrated charge and current preamplifier coupled with high granularity silicon detectors," *Nuclear Instruments and Methods in Physics Research, Section A: Accelerators, Spectrometers, Detectors and Associated Equipment*, vol. 1013, 2021.

[4] A. Pullia, G. Pascovici, B. Cahan, D. Weisshaar, C. Boiano, R. Bassini, M. Petcu, and F. Zocca, "The AGATA charge-sensitive preamplifiers with built-in active-reset device and pulser," in *IEEE Symposium Conference Record Nuclear Science 2004.*, vol. 3. IEEE, 2004, pp. 1411–1414.

[5] S. Capra, D. Mengoni, R. Aliaga, A. Gadea, and A. Pullia, "Experimental performance of the I^2C integrated multichannel charge-sensitive preamplifier of TRACE," 2016.

[6] M. Pfützner *et al.*, "Charged-particle spectroscopy in the microsecond range following projectile fragmentation," *Nuclear Instruments and Methods in Physics Research, Section A: Accelerators, Spectrometers, Detectors and Associated Equipment*, vol. 493, no. 3, pp. 155–164, 2002.

[7] G. L. Montagnani, L. Buonanno, D. Di Vita, C. Fiorini, and M. Carminati, "A compact 4-decade dynamic range readout module for gamma spectroscopy and imaging," in *2019 IEEE International Symposium on Circuits and Systems (ISCAS)*, 2019, pp. 1–5.

[8] F. Crespi *et al.*, "Response of AGATA segmented HPGe detectors to gamma rays up to 15.1 MeV," *Nucl. Instrum. Methods Phys. Res. A: Accel. Spectrom. Detect. Assoc. Equip.*, vol. 705, pp. 47–54, 2013.

[9] D. Schneiders *et al.*, "Position-sensitive detection of cosmic radiation in a segmented HPGe detector," *Verhandlungen der Deutschen Physikalischen Gesellschaft*, 2014. [Online]. Available: http://www.dpg-verhandlungen.de

[10] D. Schneiders, *Detection of high-energy muons from cosmic rays with a highly-segmented HPGe detector*, 2014. [Online]. Available: https://www.ikp.uni-koeln.de/fileadmin/data/reiter/theses/schneiders{_}master.pdf

[11] R. Kumar *et al.*, "Testing of a dsssd detector for the stopped rising project," *Nucl. Instrum. Methods Phys. Res. A: Accel. Spectrom. Detect. Assoc. Equip.*, vol. 598, no. 3, pp. 754–758, 2009.

[12] "The GRIT project." [Online]. Available: https://www.in2p3.cnrs.fr/sites/institut_in2p3/files/page/2019-07/9-Doc-BEAUMEL.pdf

[13] S. Riboldi, A. Pullia, F. Zocca, D. Budjas, A. Andragora, and C. M. Cattadori, "Test of a fully integrated CMOS preamplifier for HPGe detectors," 11 2008, pp. 2071 – 2073.

[14] S. Capra, D. Mengoni, R. Aliaga, A. Gadea, V. Gonzalez, and A. Pullia, "Design of an integrated low-noise, low-power charge sensitive preamplifier for γ and particle spectroscopy with solid state detectors," 2016.

[15] S. Capra, "Impedance and noise closed-form model of large-area integrated resistors with high stray capacitance to be used as feedback discharge devices in charge-sensitive preamplifiers for nuclear spectroscopy," *IEEE Transactions on Nuclear Science*, vol. 67, no. 4, pp. 722–731, 2020.

[16] S. Capra and A. Pullia, "Study of the effects of parasitic capacitance on large integrated feedback resistors for charge-sensitive preamplifiers," *2014 IEEE Nuclear Science Symposium and Medical Imaging Conference, NSS/MIC 2014*, 2016.

[17] E. Monteil *et al.*, "A prototype of a new generation readout ASIC in 65 nm CMOS for pixel detectors at HL-LHC," *Journal of Instrumentation*, vol. 11, no. 12, pp. C12 044–C12 044, dec 2016.

[18] A. Pullia and S. Capra, "Experimental performance of a highly-innovative low-noise charge-sensitive preamplifier with integrated range-booster," *Journal of Instrumentation*, vol. 13, no. 12, 2018.

[19] S. Capra and A. Pullia, "Design and experimental validation of an integrated multichannel charge amplifier for solid-state detectors with innovative spectroscopic range booster," *IEEE Transactions on Nuclear Science*, vol. 67, no. 8, pp. 1877–1884, 2020.

[20] A. Pullia, F. Zocca, and S. Capra, "Note: A 102 dB dynamic-range charge-sampling readout for ionizing particle/radiation detectors based on an application-specific integrated circuit (asic)," *Review of Scientific Instruments*, vol. 89, no. 2, 2018.

[21] S. Capra *et al.*, "Performance of the new integrated front-end electronics of the TRACE array commissioned with an early silicon detector prototype," *Nucl. Instrum. Methods Phys. Res. A: Accel. Spectrom. Detect. Assoc. Equip.*, vol. 935, pp. 178–184, 2019.

[22] M. Siciliano, J. Ljungvall, A. Goasduff, A. Lopez-Martens, M. Zielińska, AGATA, and O. collaborations, "Position uncertainties of AGATA pulse-shape analysis estimated via the bootstrapping method," *European Physical Journal A*, vol. 57, no. 2, 2021.

[23] N. Cieplicka-Oryńczak *et al.*, "Towards the lowest-energy limit for light ions identification with silicon pixel-type detectors," *European Physical Journal A*, vol. 54, no. 12, 2018.

[24] R. Aliaga *et al.*, "Conceptual design of the TRACE detector readout using a compact, dead time-less analog memory ASIC," *Nucl. Instrum. Methods Phys. Res. A: Accel. Spectrom. Detect. Assoc. Equip.*, vol. 800, pp. 34–39, 2015.